

Creasing-wrinkling transition in elastomer films under electric fields

Qiming Wang and Xuanhe Zhao*

*Soft Active Materials Laboratory, Department of Mechanical Engineering and Materials Science,
Duke University, Durham, North Carolina 27708, USA*

(Received 10 June 2013; published 9 October 2013)

Creasing and wrinkling are different types of instabilities on material surfaces characterized by localized singular folds and continuously smooth undulation, respectively. While it is known that electric fields can induce both types of instabilities in elastomer films bonded on substrates, the relation and transition between the field-induced instabilities have not been analyzed or understood. We show that the surface energy, modulus, and thickness of the elastomer determine the types, critical fields, and wavelengths of the instabilities. By independently varying these parameters of elastomers under electric fields, our experiments demonstrate transitions between creases with short wavelengths and wrinkles with long wavelengths. We further develop a unified theoretical model that accounts for both creasing and wrinkling instabilities induced by electric fields and predicts their transitions. The experimental data agree well with the theoretical model.

DOI: [10.1103/PhysRevE.88.042403](https://doi.org/10.1103/PhysRevE.88.042403)

PACS number(s): 68.55.J-, 82.35.Lr, 61.41.+e, 77.84.Jd

I. INTRODUCTION

When an elastomer film constrained on a substrate is subject to an electric field, the initially flat surface of the elastomer can bifurcate into two distinct modes of instabilities: (i) creases or dimples characterized by localized singular regions of self-contact [1,2], or (ii) wrinkles characterized by continuously smooth undulation [3–8]. The electric-field-induced creasing and wrinkling instabilities have been widely implicated in detrimental failures of insulating cables [9,10], organic capacitors [11], and dielectric-elastomer actuators [2,12] and energy harvesters [13]. Conversely, controlling these instabilities with electric fields has led to beneficial applications as diverse as functional surfaces and interfaces [3,4], biomedical devices [14], and on-demand patterning [15]. Since the pioneering work by Biot [16], existing studies on creasing and wrinkling instabilities have been mostly focused on elastomers under mechanical loads [17–22]. On the other hand, the relation and transition between creasing and wrinkling instabilities caused by applying physical fields, such as electric fields, have not been analyzed or understood. However, such an understanding is of timely importance to both physics and technological applications of instabilities in soft materials [3,4,14,15].

Here we present a comparative study on the creasing and wrinkling instabilities in substrate-bonded elastomers subject to electric fields. By combining theory and experiments, we show that the surface energy γ , shear modulus μ , and thickness H of the elastomer determine the electric-field-induced instabilities: A ratio between the surface energy and shear modulus of the elastomer defines a material-specific length scale, i.e., elastocapillary length γ/μ [23–28]. If the elastocapillary length is larger than the thickness of the elastomer film, the wrinkling instability sets in the elastomer under electric fields [4,5]. If the elastocapillary length is comparable to or smaller than the film thickness, the creasing instability occurs at localized regions on the elastomer surface.

Transitions between wrinkling and creasing can be achieved by independently varying an elastomer's surface energy, shear modulus, or thickness. In elastomers with the same thickness, the wavelength of the wrinkles is much larger than that of the corresponding creases.

II. EXPERIMENT

The experimental setup in the current study is illustrated in Figs. 1(a) and 1(b) [2,4,12]. A layer of a silicone elastomer (Sylgard 184, Dow Corning, USA) was bonded on a rigid polymer substrate (Kapton, DuPont, USA) by spin-coating and then curing at 65 °C for 12 h. Elastomer films with thickness from $10 \pm 2 \mu\text{m}$ to $59 \pm 4 \mu\text{m}$ were obtained by varying the spin-coating speed. The shear modulus of the rigid substrate was measured to be $\sim 50 \text{ GPa}$, and that of the elastomer varied from $\sim 161 \text{ Pa}$ to 155 kPa by varying the elastomer's cross-link density (Fig. S1(d) in Supplemental Material [29]). The top surface of the elastomer film was immersed in 10 wt % NaCl solution, which acted as a transparent flexible electrode [2,12]. The surface energy of silicone elastomer in NaCl solution is $\sim 0.04 \text{ N/m}$ [30], but can be reduced to 0.0047 N/m by adding a surfactant (Triton X-100, EMD Chemicals, USA) in the solution above its critical micelle concentration [31]. A direct-current voltage (Mastsusada, Japan) was applied between the NaCl solution and a metal plate bonded on the substrate with a ramping rate of 10 V/s , until instabilities occurred on the elastomer. The instabilities were recorded by an optical microscope lens connected with a camera (Nikon, Japan).

Figures 1(c)–1(f) give a set of electric-field-induced instabilities observed on surfaces of elastomers with the same surface energy $\gamma = 0.04 \text{ N/m}$ and thickness $H = 10 \pm 2 \mu\text{m}$, but different shear moduli μ ranging from 161 Pa to 38 kPa . When the elastocapillary length is smaller than the film thickness, i.e., $\gamma/(\mu H) = 0.1$, a sufficiently high electric field induces the creasing instability on the elastomer surface as localized folds with a wavelength $\lambda \approx 1.5H$ [Fig. 1(c)]. To validate the creases are concave and localized, the surface topography of a highly deformed Sylgard film by electric field was characterized by atomic force microscopy (AFM)

*Author to whom correspondence should be addressed: xz69@duke.edu

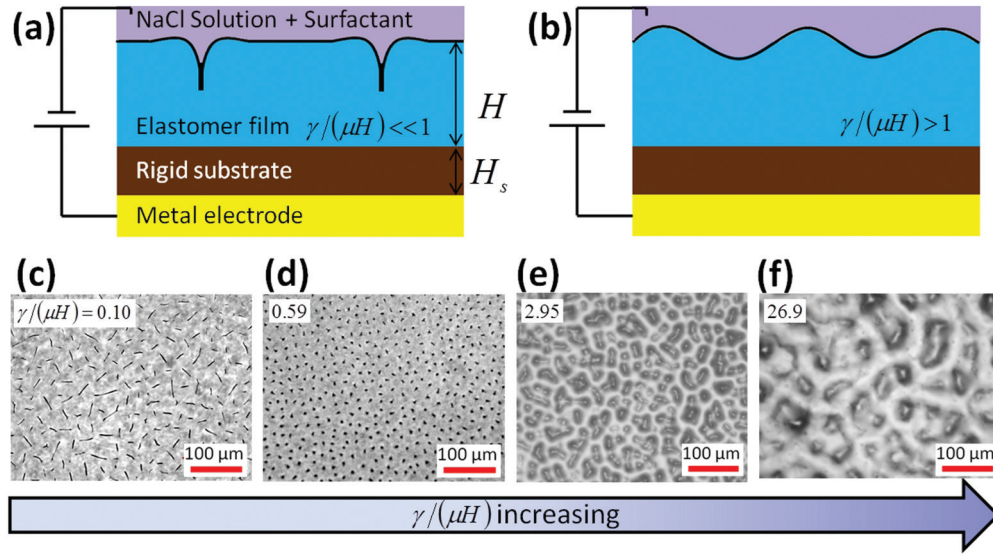


FIG. 1. (Color online) Schematic illustration of the experimental setup to induce the creasing (a) and wrinkling (b) instabilities in elastomers bonded on substrates with electric fields. The instabilities generated in elastomer films with the same thickness $H = 10 \pm 2 \mu\text{m}$ and surface energy $\gamma = 0.04 \text{ N/m}$ but different shear moduli μ : 38 173 Pa (c), 6719 Pa (d), 1358 Pa (e), and 161 Pa (f).

(Fig. S2 [29]). In contrast, when $\gamma/(\mu H) = 26.9$, the wrinkling instability occurs as smooth surface undulations with much longer wavelengths, $\lambda \approx 10H$ [Fig. 1(f)]. As the shear modulus of the elastomer decreases, a transition from the creasing to wrinkling instabilities can be observed [Figs. 1(c)–1(f)].

III. THEORY

The experimental observations are qualitatively understood as follows. The potential energy of the system (i.e., elastomer and applied voltage) can be expressed as $\Pi = U_E + U_M + U_S$, where U_E is the electrostatic potential energy of the system, and U_M and U_S the elastic and surface energies of the elastomer, respectively. While the flat state of the elastomer gives the lowest elastic and surface energies, the wrinkled or creased state has lower electrostatic potential energy than the flat state. Therefore, the decrease of the system's electrostatic potential energy drives the wrinkling and creasing instabilities, which are resisted by the increase of elastic and surface energies of the elastomer. Depending on whether the surface or elastic energy is dominant, the preferred mode of instability is either wrinkling or creasing, respectively.

To quantitatively explain the phenomena, we develop a unified theoretical model to account for both wrinkling and creasing instabilities in elastomers under electric fields and predict their transitions. For simplicity, we restrict our analyses to plane-strain deformation of the elastomer. Because the low ramping rate of the voltage approximates a quasistatic loading, the elastomer is taken as an incompressible neo-Hookean material with negligible viscoelastic effect [29]. Stress equilibrium in the elastomer requires $\nabla \cdot \boldsymbol{\sigma} = 0$, where the total stress in the elastomer consists of the mechanical and electrical stresses, i.e., $\boldsymbol{\sigma} = \boldsymbol{\sigma}_M + \boldsymbol{\sigma}_E$. For a neo-Hookean material, the mechanical stress can be expressed as $\boldsymbol{\sigma}_M = \mu \mathbf{F}\mathbf{F}^T - p\mathbf{I}$, where \mathbf{F} is the deformation gradient tensor and \mathbf{F}^T the transpose of \mathbf{F} , p the hydrostatic pressure, and \mathbf{I}

the unit tensor. The electrical stress in the elastomer can be expressed as $\boldsymbol{\sigma}_E = \varepsilon \mathbf{E}\mathbf{E} - \varepsilon(\mathbf{E} \cdot \mathbf{E})\mathbf{I}/2$, where ε is the electric permittivity of the elastomer and \mathbf{E} the electric-field vector in the elastomer [32,33]. On the top surface of the elastomer, the Young-Laplace relation prescribes $\boldsymbol{\sigma} \cdot \mathbf{n} = 2\gamma\boldsymbol{\kappa}\mathbf{n}$, where $\boldsymbol{\kappa}$ is the mean curvature of the top surface, while the displacement on the bottom surface of the elastomer is 0. When the elastomer is at flat state, the deformation and electric fields are homogeneous, i.e., $\mathbf{F} = \mathbf{I}$ and $\mathbf{E} = [0 \ E]^T$, where E is the applied electric field in the elastomer film.

A. Wrinkling instability

We now analyze the electric-field-induced wrinkling instability with a linear perturbation method following [7], given that the initiation of wrinkling only involves small deformation of the elastomer [29]. The bifurcated wrinkled state is required to satisfy the equilibrium and boundary conditions described above. Consequently, we find that the applied electric field to induce the wrinkling instability depends on the wavelength of the wrinkles via [7]

$$\frac{\varepsilon E^2}{\mu} = 2Hk \frac{1 + 2e^{2Hk} + e^{4Hk} + 4e^{2Hk}H^2k^2}{-1 + e^{4Hk} - 4e^{2Hk}Hk} + (Hk)^2 \frac{\gamma}{\mu H}, \quad (1)$$

where k is the wave number which gives the corresponding wavelength of the wrinkle $\lambda = 2\pi H/k$. Based on Eq. (1), we plot the normalized electric field $E\sqrt{\varepsilon/\mu}$ as functions of Hk for various $\gamma/(\mu H)$ in Fig. 2(a). The lowest electric field on each curve in Fig. 2(a) gives the critical electric field for wrinkling in an elastomer with a specific value of $\gamma/(\mu H)$, as well as the corresponding wavelength (or wave number) of the wrinkle. We find the critical electric field is $\sim 2.49\sqrt{\mu/\varepsilon}$ when $\gamma = 0$; thereafter the critical field increases approximately

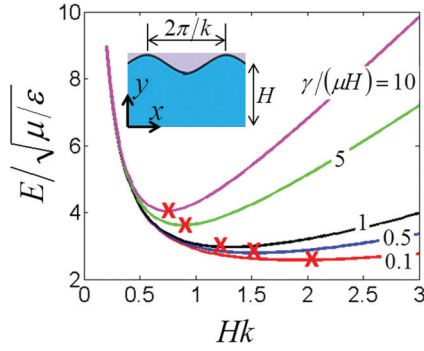


FIG. 2. (Color online) The calculated electric field for inducing the wrinkling instabilities in elastomers with various values of $\gamma/(\mu H)$. The lowest electric field in each curve gives the critical electric field for wrinkling instability.

linearly with $\sqrt{\gamma/(H\varepsilon)}$, i.e.,

$$E_{\text{wrinkle}}^c \approx 2.49\sqrt{\frac{\mu}{\varepsilon}} + 0.46\sqrt{\frac{\gamma}{H\varepsilon}}. \quad (2)$$

It is noted that if the elastomer is taken to be a viscoelastic solid, the calculated critical electric field for the wrinkling instability is the same as Eq. (2) [29].

B. Creasing instability

We next analyze the creasing instability in the elastomer under electric fields. Since the formation of creases involves large deformation and singular electric field, the linear perturbation method is not applicable here. Instead, we compare the potential energy between the flat and creased states [2,21,34]. The analysis domain is shown in the inset of Fig. 3(a). For simplicity, the rigid substrate is not included in the current analysis. The width of the domain w is taken as a wavelength of the crease pattern under plane-strain deformation [15]. Due to symmetry of the crease, only half of the region is analyzed. Considering the elastomer as an isotropic ideal dielectric [32], the total potential energy of the system (unit length in the third direction) can be expressed as

$$\begin{aligned} \Pi = U_E + U_M + U_S = & - \int_S \frac{1}{2} \varepsilon |\mathbf{E}|^2 dS \\ & + \int_S W_M dS + \int_L \gamma dL, \end{aligned} \quad (3)$$

where W_M is the elastic energy density in the elastomer, S is the area of the elastomer domain, and L the contour of the top free surface of the elastomer (i.e., the interface between the elastomer and the top electrode). To calculate the critical electric field for the creasing instability, we compare the potential energy between the creased and flat states.

At the flat state, considering the incompressibility of the elastomer, the bottom-constrained film does not undergo any deformation. The electric field in the elastomer film is $E = \Phi/H$, and the potential energy of the system at flat state is

$$\Pi_{\text{flat}} = -\frac{1}{2} \varepsilon E^2 H w + \gamma w. \quad (4)$$

At the creased state, the elastomer surface folds against itself to form a segment of self-contact with length a . We use

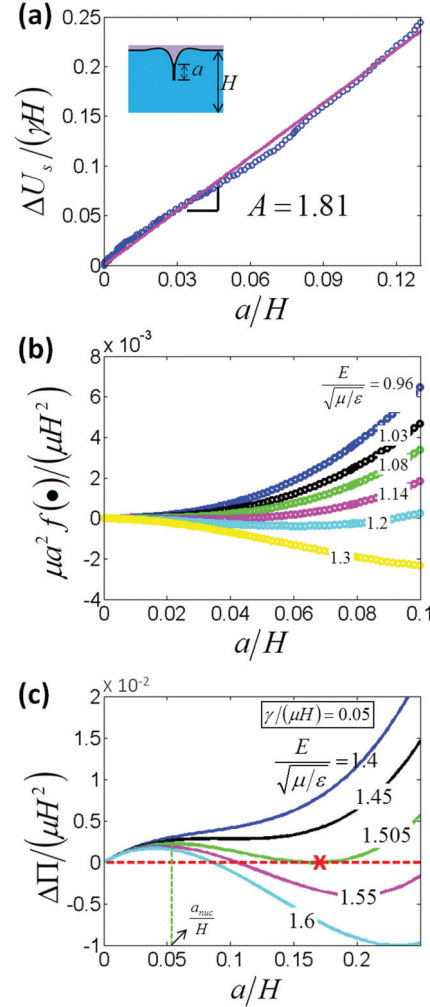


FIG. 3. (Color online) Surface-energy difference (a) and the electroelastic potential energy difference (b) between creased and flat states calculated by the finite-element model. (c) The calculated potential energy difference between the creased and flat states $\Delta\Pi$ for an elastomer with $\gamma/(\mu H) = 0.05$ under various electric fields. The electric field that satisfies $\Delta\Pi = 0$ and $\partial\Delta\Pi/\partial(a/H) = 0$ gives the critical electric field for the creasing instability.

a finite-element model based on software, ABAQUS 6.10.1, to calculate the potential energy of the elastomer at the creased state [2]. In order to maintain the convergence of the numerical model, we neglect the effect of surface energy on the shape of the crease [21]. The calculated surface-energy difference between the creased and flat states is plotted in Fig. 3(a). The surface-energy difference is found to be approximately linearly related to the crease size a , i.e., $\Delta U_S = A a \gamma$, where $A \approx 1.81$. Therefore, by dimensional analysis, the potential energy difference between the creased and flat state can be expressed as [21]

$$\Delta\Pi = \mu a^2 f(E\sqrt{\varepsilon/\mu}, a/H) + A \gamma a, \quad (5)$$

where $f(\bullet)$ is a nondimensional function that characterizes the electric and elastic potential energy difference between creased and flat states. The calculated function $\mu a^2 f(\bullet)$ is plotted in Fig. 3(b). In Fig. 3(c) we plot $\Delta\Pi$ as functions of a/H for

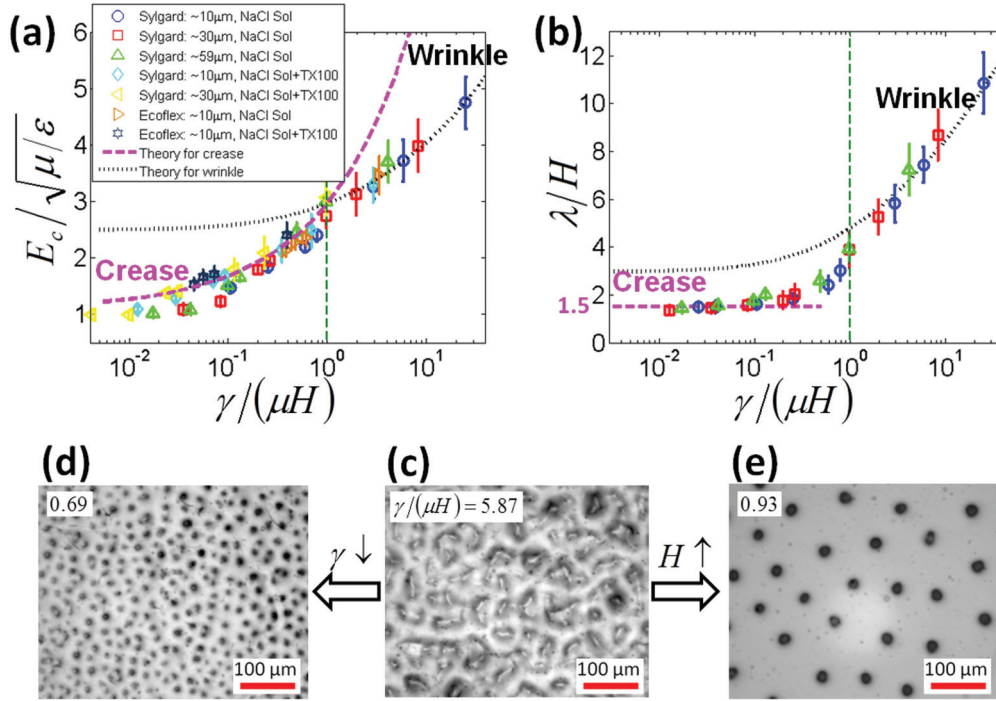


FIG. 4. (Color online) The critical electric fields (a) and wavelengths (b) for wrinkling and creasing instabilities predicted by the theoretical model and observed in experiments. The wrinkling instability in an elastomer with $\gamma = 0.04$ N/m, $H = 10$ μ m, and $\mu = 681$ Pa (c) can be transitioned to the creasing instability by independently decreasing the elastomer's surface energy to $\gamma = 0.0047$ N/m (d) or increasing its thickness to $H = 63$ μ m (e).

$\gamma/(\mu H) = 0.05$ and various values of $E\sqrt{\epsilon/\mu}$. The formation of crease requires $\Delta\Pi = 0$ and $\partial\Delta\Pi/\partial(a/H) = 0$, the solving of which gives the critical electric field for $\gamma/(\mu H) = 0.05$ as shown in Fig. 3(c). In general, the critical electric field for creasing instability can be approximately calculated as a function of μ , γ , and H , i.e.,

$$E_{\text{crease}}^c \approx 1.03\sqrt{\frac{\mu}{\epsilon}} + 1.88\sqrt{\frac{\gamma}{H\epsilon}}. \quad (6)$$

When $\gamma = 0$, Eq. (6) recovers the critical electric field for creasing instability on elastomers without surface energy, i.e., $1.03\sqrt{\mu/\epsilon}$ [2]. It should be noted that the critical electric field predicted by Eq. (6) is for the growth of creases [21]. Correspondingly, the measured critical field in experiment [Fig. 4(a)] is also the electric field that generates a pattern of creases in the film (i.e., for growth of creases). In addition, a comparison between Figs. 3(b) and 3(c) shows that the surface energy introduces an energy barrier for the nucleation and growth of creases under the critical electric field [21]. Random defects and surface roughness over a critical size a_{nuc} can facilitate the elastomer to exceed the energy barrier [21]. For example, Fig. 3(c) shows that defects with size on the order of $0.05H$ will enable the nucleation and growth of creases under the critical electric field. Figure S3 [29] further gives the critical defect sizes to nucleate and grow creases under critical electric fields in elastomers with various values of $\gamma/(\mu H)$. Since the defects and roughness of elastomers usually cannot be well controlled in experiments, the measured critical electric

fields from different samples may slightly deviate from the theoretical prediction and each other, as shown in Fig. 4(a).

IV. RESULTS AND DISCUSSIONS

A combination of the theories for wrinkling and creasing instabilities under electric field can predict the transition between the two types of instabilities. We plot Eqs. (2) and (6) in Fig. 4(a). This combination predicts that the wrinkling instability has lower critical field and thus sets in when $\gamma/(\mu H) > 1$, while the creasing has lower critical field when $\gamma/(\mu H) < 1$. The theoretical prediction is consistent with the experimental observations [Figs. 1(c)–1(f)]. To further validate the theory, we record the electric-field-induced instabilities in elastomer films with various thicknesses H , moduli μ , and surface energy γ [Fig. 4(a)]. For each case of $\gamma/(\mu H) > 1$, the wrinkling instability with relatively long wavelength $\lambda_{\text{wrinkle}} = 5 - 12H$ are observed. The wavelengths of the wrinkles also match well with the theoretical prediction [Fig. 4(b)]. On the other hand, when $\gamma/(\mu H) < 1$, the creasing instabilities are observed with a short wavelength $\lambda_{\text{crease}} = 1.5 - 3H$, well below the predicted wavelengths for wrinkling instability [Fig. 4(b)]. When $\gamma/(\mu H) < 0.1$, the wavelength of the creases reaches $\lambda_{\text{crease}} \approx 1.5H$, consistent with the wavelength previously observed on elastomers with negligible surface-energy effect [2]. The measured critical electric fields for both creasing and wrinkling instabilities also match consistently with the theoretical predictions [Fig. 4(a)].

The transition between wrinkling and creasing can also be achieved by independently varying the elastomer's thickness or surface energy, in addition to changing its modulus [Figs. 1(c)–1(f)]. As shown in Fig. 4(c), the wrinkling instability occurs on an elastomer film with $\gamma = 4 \times 10^{-2} \text{ N m}^{-1}$, $\mu = 681 \text{ Pa}$, and $H = 10 \text{ }\mu\text{m}$. After reducing the surface energy to $\gamma = 4.7 \times 10^{-3} \text{ N m}^{-1}$ with surfactant, the creasing instability sets in the same elastomer as localized dimples with a wavelength much smaller than the corresponding wrinkles, since $\gamma/(\mu H)$ has been reduced to 0.69 [Fig. 4(c)]. Furthermore, we increase the thickness of the elastomer to $H \approx 63 \text{ }\mu\text{m}$, while maintaining $\gamma = 4 \times 10^{-2} \text{ N m}^{-1}$ and $\mu = 681 \text{ Pa}$. Since $\gamma/(\mu H)$ reaches 0.93, the creasing instability sets in once again but with a wavelength larger than the previous one, due to the increased film thickness. We also observe similar transitions between creasing and wrinkling instabilities in a different elastomer, Ecoflex (Smooth-On, USA), illustrating the generality of the theory (Fig. S4 [29]).

Notably, the creasing-wrinkling transition has not been observed in elastomers under mechanical compression, where the creasing instability is preferable for all values of $\gamma/(\mu H)$ [21]. This discrepancy is due to the differences in the loads and boundary conditions that the elastomers are subjected to between previous and current studies. In previous studies, the creasing instability is formed on mechanically compressed elastomer films, which have been homogeneously deformed prior to the instability. On the other hand, the wrinkling or creasing in the current work is induced by electric field in a substrate-bonded elastomer film, which maintains undeformed until the instability sets in. Therefore, the contributions from elastic and surface energies to the instabilities can be significantly different in previous and current studies, depending on whether the elastomer is homogeneously deformed or not. For example, the surface-energy difference between the creased state and the flat state in the current work is $\sim 1.81a\gamma$, but it is only $\sim 0.45a\gamma$ for elastomer films under mechanical compression [21]. Consequently, for elastomers under mechanical compression, the critical compressive strain for the creasing instability is always lower than that for the corresponding wrinkling instability. On the other hand, for elastomers under electric fields, the critical electric field for creasing instability is lower when $\gamma/(\mu H) < 1$, but that for wrinkling instability is lower when $\gamma/(\mu H) > 1$.

We further explore the postbehaviors of electric-induced creasing and wrinkling instabilities. While it is known that the electric-field-induced creases can be further deformed into craters [2], the postwrinkling morphology of elastomers immersed in liquid electrodes is still not clear. In Video S1 [29], we give the electric-field-induced evolution of the surface morphology of an elastomer with $\gamma/(\mu H) = 1333$ (it should be noted that the elastomer is in a liquidlike state here, since its storage modulus is lower than the loss modulus, as shown in Fig. S1(a) [29]). Under a ramping electric field, the initial wrinkles in the elastomer quickly localize into ridges, which are further deformed into domains with a spherical shape [Video S1 [29] and Fig. 5(a)]. To better image the evolution of the instability patterns, we apply electric fields on partially cured elastomers to induce instabilities and then cure the elastomers in the postwrinkling states. Thereafter, the

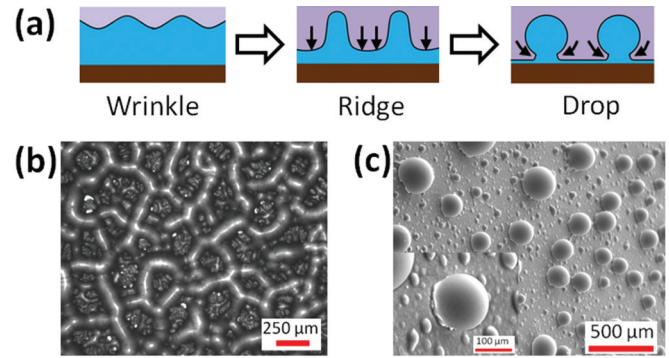


FIG. 5. (Color online) Schematic illustrations of the electric-field-induced wrinkles evolving into localized ridges and drops (a). Optical and scanning-electron microscope images of the ridges (b) and drops (c) evolved from the wrinkles.

cured elastomers are imaged with optical or scanning-electron microscopes. Figure 5(b) shows that the wrinkles in the partially cured elastomers first evolve into ridges with their valleys pushed down onto the surface of the rigid substrate. This is because the electric field and therefore electric stress are higher at the valley regions of the wrinkles than the peak regions. The higher electric stress tends to push the valleys further down, leading to a pattern of ridges [Figs. 5(a) and 5(b)]. After the ridges develop, the electric stress tends to further deform them into localized domains with a shape of drops [Figs. 5(a) and 5(c)].

V. CONCLUSIONS

In summary, we present a unified model for the electric-induced creasing and wrinkling instabilities in elastomers bonded on substrates. Depending on whether the elastocapillary length γ/μ of the elastomer is larger or smaller than its thickness H , the preferred mode of instability is the wrinkling with long wavelength or creasing with short wavelength, respectively. By independently varying the modulus μ , surface energy γ , and thickness H of elastomers, our experiments achieve transitions between wrinkling and creasing instabilities. The experimentally observed critical fields and wavelengths for the instabilities match consistently with the theoretical model. We further demonstrate that the electric-field-induced wrinkles can further evolve into localized ridges and drops. The theory and experiments presented here advance the understanding of field-induced instabilities in soft materials for diverse technological applications.

ACKNOWLEDGMENTS

This work was supported by NSF CAREER Award (CMMI-1253495) and NSF Triangle MRSEC (Grant No. DMR-1121107). X.H.Z. acknowledges the support from NSF (Grant No. CMMI-1200515). Q.M.W. acknowledges the support of a fellowship from Duke Center for Bimolecular and Tissue Engineering (Grant No. NIH-2032422).

- [1] Q. Wang, Z. Suo, and X. Zhao, *Nat. Commun.* **3**, 1157 (2012).
- [2] Q. Wang, L. Zhang, and X. Zhao, *Phys. Rev. Lett.* **106**, 118301 (2011).
- [3] M. D. Morariu, E. Schäffer, Z. Lin, T. P. Russell, and U. Steiner, *Nat. Mater.* **2**, 48 (2003).
- [4] E. Schaffer, T. Thurn-Albrecht, T. P. Russell, and U. Steiner, *Nature* **403**, 874 (2000).
- [5] N. Arun, A. Sharma, P. S. G. Pattader, I. Banerjee, H. M. Dixit, and K. S. Narayan, *Phys. Rev. Lett.* **102**, 254502 (2009).
- [6] N. Arun, A. Sharma, V. B. Shenoy, and K. S. Narayan, *Adv. Mater.* **18**, 660 (2006).
- [7] V. Shenoy and A. Sharma, *Phys. Rev. Lett.* **86**, 119 (2001).
- [8] J. Sarkar and A. Sharma, *Langmuir* **26**, 8464 (2010).
- [9] L. A. Dissado and J. C. Fothergill, *Electrical Degradation and Breakdown in Polymers* (IET, Stevenage, UK, 1992), Vol. 9.
- [10] L. Zhang, Q. Wang, and X. Zhao, *Appl. Phys. Lett.* **99**, 171906 (2011).
- [11] B. Chu, X. Zhou, K. Ren, B. Neese, M. Lin, Q. Wang, F. Bauer, and Q. M. Zhang, *Science* **313**, 334 (2006).
- [12] Q. Wang, M. Tahir, L. Zhang, and X. Zhao, *Soft Matter* **7**, 6583 (2011).
- [13] Q. Wang, X. Niu, Q. Pei, M. D. Dickey, and X. Zhao, *Appl. Phys. Lett.* **101**, 141911 (2012).
- [14] P. Shivapooja, Q. Wang, B. Orihuela, D. Rittschof, G. P. López, and X. Zhao, *Adv. Mater.* **25**, 1430 (2013).
- [15] Q. Wang, M. Tahir, J. Zang, and X. Zhao, *Adv. Mater.* **24**, 1947 (2012).
- [16] M. A. Biot, *Appl. Sci. Res., Sect. A* **12**, 168 (1963).
- [17] E. Hohlfeld and L. Mahadevan, *Phys. Rev. Lett.* **106**, 105702 (2011).
- [18] E. Hohlfeld and L. Mahadevan, *Phys. Rev. Lett.* **109**, 025701 (2012).
- [19] T. Tallinen, J. S. Biggins, and L. Mahadevan, *Phys. Rev. Lett.* **110**, 024302 (2013).
- [20] S. Cai, D. Chen, Z. G. Suo, and R. C. Hayward, *Soft Matter* **8**, 1301 (2012).
- [21] D. Chen, S. Cai, Z. Suo, and R. C. Hayward, *Phys. Rev. Lett.* **109**, 038001 (2012).
- [22] A. Ghatak and A. L. Das, *Phys. Rev. Lett.* **99**, 076101 (2007).
- [23] B. Roman and J. Bico, *J. Phys.: Condens. Matter* **22**, 493101 (2010).
- [24] A. Ghatak, M. K. Chaudhury, V. Shenoy, and A. Sharma, *Phys. Rev. Lett.* **85**, 4329 (2000).
- [25] J. Bico, B. Roman, L. Moulin, and A. Boudaoud, *Nature* **432**, 690 (2004).
- [26] J. Huang, J. Liu, B. Kroll, K. Bertoldi, and D. R. Clarke, *Science* **317**, 650 (2007).
- [27] A. Jagota, D. Paretkar, and A. Ghatak, *Phys. Rev. E* **85**, 051602 (2012).
- [28] X. Xu, A. Jagota, S. Peng, D. Luo, M. Wu, and C.-Y. Hui, *Langmuir* **29**, 8665 (2013).
- [29] See Supplemental Material at <http://link.aps.org/supplemental/10.1103/PhysRevE.88.042403> for four additional figures and linear stability analysis of electrowrinkling instability.
- [30] A. G. Kanellopoulos and M. J. Owen, *Trans. Faraday Soc.* **67**, 3127 (1971).
- [31] K. G. Marinova, D. Christova, S. Tcholakova, E. Efreimov, and N. D. Denkov, *Langmuir* **21**, 11729 (2005).
- [32] X. Zhao, W. Hong, and Z. Suo, *Phys. Rev. B* **76**, 134113 (2007).
- [33] X. Zhao and Z. Suo, *Appl. Phys. Lett.* **91**, 061921 (2007).
- [34] W. Hong, X. Zhao, and Z. Suo, *Appl. Phys. Lett.* **95**, 111901 (2009).